

## Validation of Three-Dimensional Simulation of Flow through Hypersonic Air-breathing Engine

Thangadurai Murugan<sup>\*1</sup>, Sudipta De<sup>1</sup> and V. Thiagarajan<sup>#</sup>

<sup>1</sup>Central Mechanical Engineering Research Institute, Durgapur - 713 209, India

<sup>#</sup>Defence Research and Development Laboratory, Hyderabad - 500 058, India

\*E-mail: murugan.thangadurai@gmail.com

### ABSTRACT

The flow path of a conceptual hypersonic air-breathing scramjet engine integrated with the vehicle (without combustion) has been simulated numerically using ANSYS CFX software with the SST turbulence model. The computations were performed for the free stream Mach number of 6 and angle-of-attack of 5°. A strong separation bubble was observed on the bodyside wall in the internal compression region where the reflected cowl shock impinges on body which in turn increases the static pressure substantially. The external-internal flow field of the hypersonic mixed compression intake, shock-boundary layer interactions, and the shock-shock interactions present in the internal compression region have qualitatively been obtained and analysed. The variation of centreline pressure along the bodyside wall close to the symmetry plane obtained from numerical simulation centreline has been compared with the experimentally measured data. It has been observed that the computed wall pressure matches fairly well with the measured values in the external ramp compression region, internal compression region and in the combustion chamber. The flow patterns and the pressure variations near the middle wall and the fuel injecting strut locations have also been analysed.

**Keywords:** Hypersonic intake, scramjet engine, numerical simulation, air-breathing engine, SST turbulence modelling

### NOMENCLATURES

$h$ (m)	Intake entry height
$M$	Mach number
$p$ (N/m <sup>2</sup> )	Pressure
$x, y, z$ (m)	Axes coordinate in three directions
$\alpha$ (deg)	Angle-of-attack
$h_{iso}$ (m)	Height of isolator (= $0.3h$ )

### Subscript

$\infty$	Free stream condition
----------	-----------------------

### 1. INTRODUCTION

Use of an air-breathing propulsion system with supersonic combustion is a key technology for improving the efficiency of a hypersonic flight vehicle. This offers an alternative to rocket-driven systems which carries both fuel and oxidizer.

Air-breathing engines have higher specific impulses than rockets and can be used in the atmosphere up to an altitude of about 30 km to 40 km. The maximum possible Mach number ( $M$ ) for various altitudes is globally mentioned in terms of dynamic pressure based on the structural limits of the flying machines<sup>1</sup>. In ramjet engines, the necessary pressure rise for the combustion is achieved by means of ramp compression. The ramjet engine is not effective for the free-stream Mach number  $M_\infty > 5$  due to high temperature at the combustion

chamber and large pressure loss is experienced in the flow path. Hence, supersonic combustion ramjet (scramjet) engine is used for hypersonic vehicles operated beyond the Mach number 5.

The scramjet engine development involves many technological challenges. This includes the thermal load management, addition of fuel to the high speed stream, mixing, ignition, flame holding, interaction between the intake and combustor and the related intake unstart issues. The concept of supersonic combustion came into limelight in the early 1950s and it was performed on aerofoil's external streams by burning fuel to either reduce the base drag or increase the lift and thrust of projectiles<sup>2</sup>. The first successful demonstration of scramjet was done by Ferri<sup>3</sup> in 1960. NASA initiated the hypersonic ramjet experiment (HRE) through X-15 Program in 1964. McClinton<sup>4</sup>, *et al.* divided the scramjet development in the United States in terms of generations. Each generation had its unique contributions on the level of understanding of scramjet combustion. Further details about the scramjet development are found in the review papers of Curran<sup>5</sup> and Fry<sup>6</sup>.

The hypersonic air-breathing technology seems to be providing large scope for the future air and space transports. Therefore, this technology is being developed worldwide. In India, the design and development of hypersonic air-breathing propulsion system is steadily taking shape at the DRDO through the Hypersonic Demonstration Vehicle Project. The

demonstration vehicle is conceptualised for an autonomous flight with a scramjet engine using the hydrocarbon fuel for less than half minute flight duration. The test article will be taken to the cruise altitude of 30 km to 32 km using the existing rocket booster and the scramjet operation will be performed at  $M_\infty = 6$ . This scramjet-integrated vehicle configuration has been designed considering the aero-propulsion interactions<sup>7</sup>.

A successful demonstration of hypersonic flight depends strongly on the functionality of the intake system and its ability to capture and compress the incoming air with less pressure loss<sup>8</sup>. Hence, air-intake is one of the crucial sub-systems in the scramjet engine. Numerous studies on hypersonic intakes have been performed for the last few decades. Bissinger<sup>9</sup>, *et al.* studied the influence of forebody shape on intake characteristics using CFD simulation for the Mach numbers ranging from 3 to 7. Their study revealed that the flat bottomed forebody with a length to width ratio of around 6.5 guaranteed a uniform flow at the entrance for angle-of-attack ( $\alpha$ ) up to  $10^\circ$ . Smart<sup>10</sup> performed the wind tunnel testing of a hypersonic intake with rectangular-to-elliptical shape transition. He observed that the intake self-started at Mach 6.2 and the Kantrowitz<sup>11</sup> self-starting limit is not applicable for this configuration. Parikh<sup>12</sup>, *et al.* performed a CFD study on X-43A stack configuration using TetrUSS software in support of the aerodynamic database generation in the transonic-to-hypersonic flow regime. They found an excellent match between the computed and the test data over a range of flow conditions. Lanson and Stollery<sup>13</sup> performed a number of hypersonic intake studies in the Cranfield Gun Tunnel for Mach No 8.2. They investigated the effect of cowl position, Reynolds number, and tripping of the boundary layer on intake performance. They found that a tripping flow with wire of 2 mm thickness improves the intake starting. Sivakumar and Babu<sup>14</sup> examined the characteristics of hypersonic intake using a commercial ANSYS Fluent software for  $M=6.5$  with various angle-of-attack conditions. They found that the flow distortion at the intake exit was quite high for angle-of-attack other than the designed condition. Saha and Chakraborty<sup>15</sup> validated the hypersonic intake starting characteristics using a 3-D simulation with Shear-Stress Transport (SST) turbulence modelling in ANSYS Fluent software. The predicted wall pressure distribution and intake performance parameters matched well with the experimental data.

Many studies are also available in the literature for flow characterisation in other sub-systems of the scramjet engine, such as isolator, combustion chamber, nozzle, and

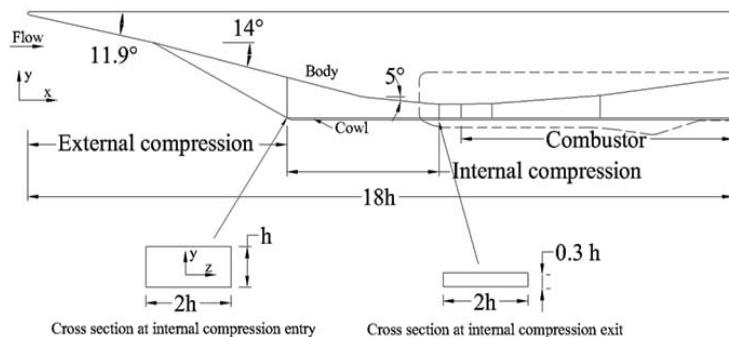


Figure 1 Intake flow path configuration.

a combination of the above sub-systems<sup>16-20</sup>. However, the flow field of the complete scramjet engine is lacking in the literature. The pressure data at the wall surfaces could be experimentally obtained through the piezo-electric transducers. However, obtaining the detailed flow structures (boundary layer, separation, vorticity, and shear layer formation) inside the scramjet engine through experiments is extremely difficult. Therefore, in the present study, a preliminary three-dimensional numerical simulation of conceptual scramjet engine has been performed using ANSYS CFX software which is a part of Analysis Program of Hypersonic Air-breathing Propulsion System of DRDO<sup>21</sup>. The main objective of the present study is to analyse the flow characteristics inside the scramjet engine of the conceptual hypersonic air-breathing vehicle.

2. INTAKE FLOW PATH

The side view of the conceptual hypersonic vehicle configuration with dimensions is shown in Fig. 1. Here, the mixed compression intake configuration is designed for  $M_\infty = 6$  with  $\alpha = 5^\circ$ . Theoretically, the two forebody ramp angles were chosen in such a way that the forebody shocks converge at the cowl lip at the designed condition. The internal compression intake has the contraction ratio (i.e., ratio of intake exit area-to-entry area) of 0.35. This conceptual vehicle had an inbuilt provision to vary the entry area of the internal compression section through a flap. A thin wall starting from the combustor entry to the exit was placed at the symmetry plane (Fig. 2). The location of this wall is shown in Fig. 1 in dashed line. The middle wall was used for improving the structural integrity of the engine. A total of eight numbers of ‘V’ shaped fuel injection struts (four on each side of the middle wall) were placed in the diverging portion of the combustor. A photograph of the scale down model of the conceptual vehicle tested in the hypersonic Mach numbers is shown in Fig. 3. The linear dimensions of the entire configuration were scaled down to suit the wind tunnel test facility requirements. The wall static pressure on body side

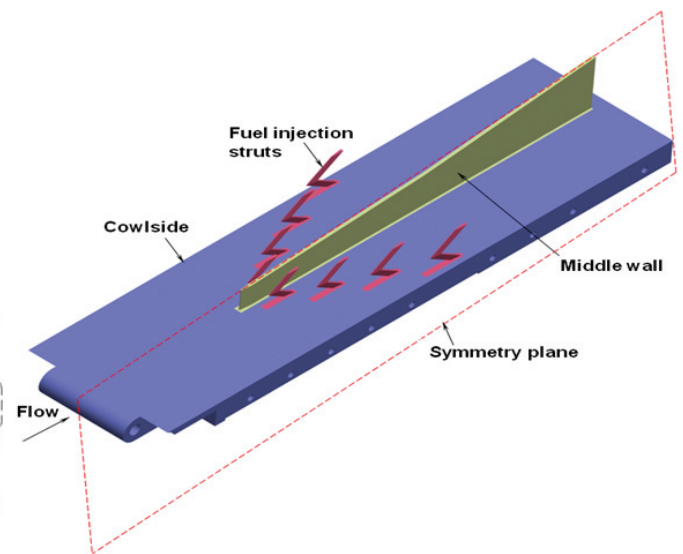


Figure 2. Middle wall and fuel injection struts arrangements on the bottom wall of combustion chamber (the portion indicated in Fig. 1 with dashed line).



Figure 3. Intake model assembled in the wind tunnel test section.

wall along the flow path was measured using multiple pressure transducers and the same was available for validating the predicted results.

### 3. COMPUTATIONAL DOMAIN AND NUMERICAL PROCEDURE

The computational domain used for the numerical simulation is shown in Fig. 4. The flow inside the scramjet engine is symmetric wrt the middle wall (Fig. 2). Hence, one half of the scramjet engine was simulated in the present study. The computational model is prepared in I-DEAS using multiple blocks. The grid generation was performed using the ANSYS ICFM CFD software. The three-dimensional flow simulation was carried out using ANSYS CFX software.

The free-stream Mach number, static pressure, temperature, and density are 6, 500.4 N/m<sup>2</sup>, 65.2 K, and 0.0267kg/m<sup>3</sup>, respectively. These are specified at the inflow boundary. Supersonic outlet condition was applied at the outflow boundary. The pressure and other flow parameters at the outflow boundary were extrapolated from the interior domain. No-slip condition is applied on all the walls (top, middle, bottom and side), cowl and on the fuel struts. The walls were considered to be in adiabatic condition. Symmetry boundary condition was applied on the middle wall plane (Fig.2). The other side boundary near the inflow was treated as a free-slip wall. A total of around 5 million cells were used in the present study. The numerical simulation was performed by solving the Navier-Stokes equation with the shear stress transport (SST) turbulence model.

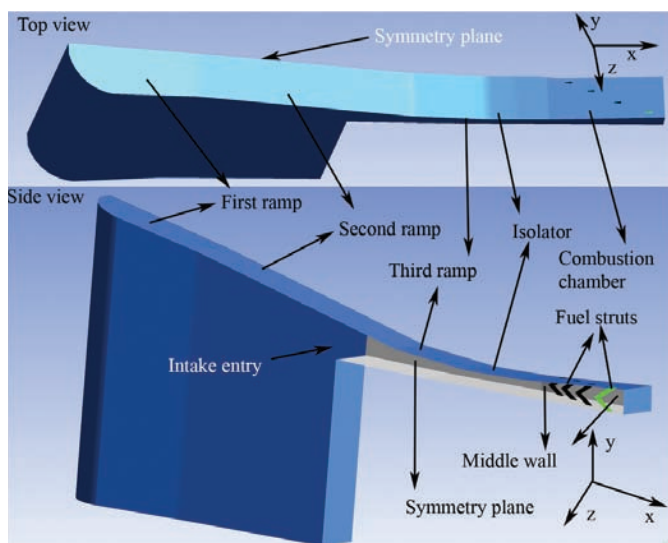


Figure 4. Computational domain.

The two-equation models are the most popular among the various available turbulence models, and offer a good compromise between complexity, accuracy, and robustness<sup>22</sup>. The standard  $k-\omega$  model of Wilcox (1998 version) has strong free-stream dependency. Menter developed the SST model that has the advantages of the Wilcox  $k-\omega$  model in the near-wall region. But, it does not have its free-stream dependency and behaves like the  $k-\epsilon$  model in the outer part of the boundary layer<sup>23</sup>. The SST model is suitable for prediction of flow separation, as in the present case, and therefore has been used in our simulation study. It should be noted that the  $k-\omega$  turbulence model has been improved by addition of the cross-diffusion term<sup>24</sup>. It does not have the free-stream sensitivity of its 1998 version<sup>25</sup>.

The residual plots of mass, momentum, and turbulence kinetic energy show good convergence of residuals. The variation of dimensionless wall boundary layer thickness ( $y^+$ ) along the non-dimensional flow axis ( $x/h$ ) on different surfaces for adiabatic wall is shown in Fig. 5. Here,  $x$  is the axial distance from nose and  $h$  is the entry height of internal compression intake. The first cell height at the bodyside wall is close to 0.083 mm. The value of  $y^+$  is less than 15 in most of the flow paths. Earlier studies<sup>14,15</sup> have shown that the  $y^+$  value of less than 40 is good enough for these simulations. A sharp rise in  $y^+$  at the cowl-leading edge was due to the formation of boundary layer at the cowl-leading edge. Similarly, a high value of  $y^+$  was observed at the leading edge of the middle wall. The fluctuations in  $y^+$  values in the combustion chamber are due to the interaction of shocks with the boundary layer.

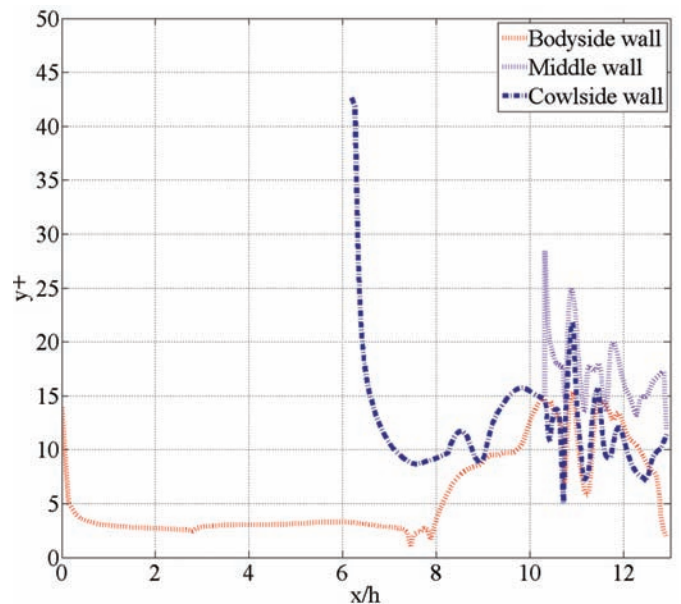


Figure 5. Variation of  $y^+$  values at bodyside, cowlside and middle wall.

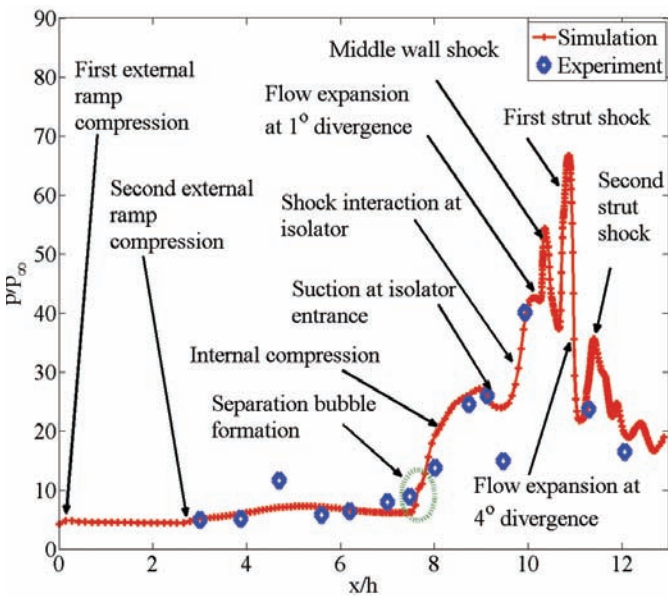
### 4. RESULTS AND DISCUSSIONS

The results obtained from numerical simulation have been validated with the experimental results at first. Next, the bodyside wall pressure distribution obtained across the lateral sections along the flow direction is presented. The flow characteristics along the engine flow path are analysed using the density gradient,  $M$ , and stream line plots in the subsequent

section. Finally, the total pressure recovery along the engine flow path is shown in addition to the sectional variation of pressure and turbulent kinetic energy (TKE).

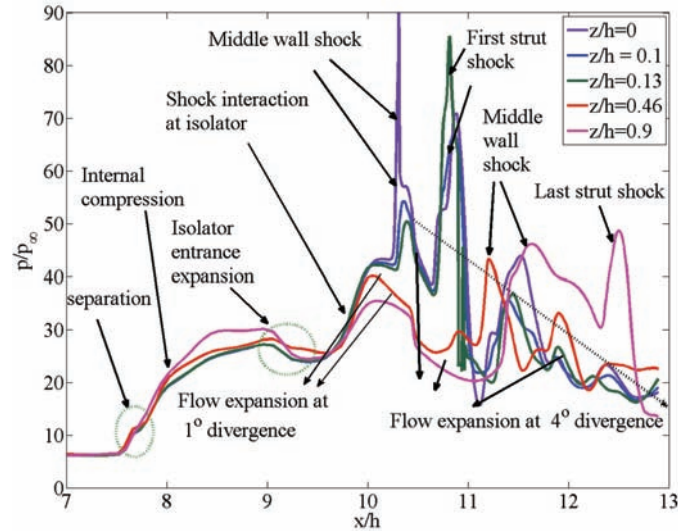
**4.1 Validation of the Numerical Results**

Figure 6 shows the variation of bodyside wall static pressure obtained from numerical simulation along with the experimental results obtained from wind tunnel experiments for  $M_\infty = 6$  with  $\alpha = 0^\circ$ . The wall pressure was normalised with the freestream static pressure. The axial length of the flow path is non-dimensionalised with the entry height of internal compression intake ( $h$ ). It is observed that the predicted wall pressure profile matches well with the experimental values in the external ramp, internal compression region, and also in the combustion chamber region. The incremental rise in pressure observed at  $x/h = 0.1$ , and 2.7 from top wall is due to the formation of weak oblique shocks at the external ramps. A sharp rise in pressure at  $x/h = 7.6$  in the internal compression region is due to the formation of a separation bubble which results from the abrupt change in flow direction at  $5^\circ$  compression ramp. The internal compression gradually increases the static pressure up to  $x/h = 9$ .



**Figure 6. Comparison of numerical results with the experimental results.**

The blunt leading edge of the middle wall acts as a stagnation point and causes sudden compression at  $x/h = 10.3$ . A strong pressure rise at  $x/h = 10.7$  is due to the interaction of oblique shock originating from the first strut with the wall. The shock from the strut interacts with the middle wall shock and creates a re-circulation zone behind the struts. This place is found to be suitable for injecting fuel so as to get better mixing of fuel and air. The shocks originating from the subsequent struts are seen from  $x/h = 11.2$  onwards. The signature of oblique shock originating from other struts continuously decreases due to the expansion of flow in the second divergence of the combustion chamber. In the region of  $x/h$  from 10 to 11, no test data is available due to constraint in the pressure measurement on the model.



**Figure 7. Variation of bodyside wall static pressure in the lateral direction.**

**4.2 Bodyside Wall Pressure Distributions**

Figure 7 illustrates the variation of bodyside wall pressure at different lateral distances along the width of the engine. Here  $z/h = 0$  represents the section on the symmetry plane (Fig. 2).  $z/h = 0.1$  and  $0.13$  represent the central plane between middle wall and the first strut and the plane along the first strut respectively.  $z/h = 0.46$  represents the central plane between middle wall (symmetry plane) and the side wall.  $z/h = 0.9$  shows central plane between the last strut and the side wall. The trend in pressure variation along the axial direction for  $z/h = 0, 0.1$  and  $0.13$  are almost similar. However, two distinct peaks at  $x/h = 10.31$  and  $10.82$  show the pressure rise due to oblique shocks emanating from the leading edge of the middle wall and the first strut.

The oblique shocks originating at other struts are not as strong as the one from the first strut. This is due to the flow expansion resulting from a divergence at the combustion chamber. Though the first and second divergence causes a continuous pressure drop at  $z/h=0.46$  and  $0.9$ , the pressure increases substantially at  $x/h = 11.2$  and  $11.5$  due to the interaction of oblique shock from the middle wall. At  $z/h=0.9$ , the reflection of shocks at the side wall causes the pressure to rise in this region of the combustion chamber. This is followed by a gradual decay till it rises again due to the shock from the last strut.

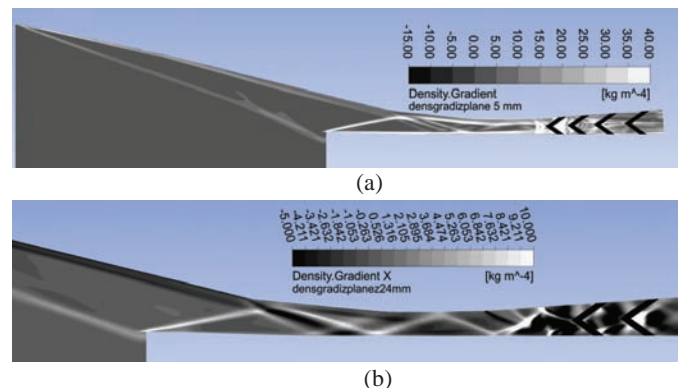


**Figure 8. Density gradient at: (a)  $z/h=0.1$  and (b)  $z/h=0.46$ .**

### 4.3 FLOW PATTERN ALONG THE ENGINE

The flow inside the scramjet engine is complex and highly shock dominated. Figure 8 show the numerical schlieren obtained at  $z/h = 0.1$  and  $z/h = 0.46$  from the symmetry plane. The forebody shocks from the nose tip and the shock from the  $14^\circ$  ramp merges just ahead of the cowl lip. It is observed that the oblique shock originating from the cowl-leading edge is much stronger than the forebody shocks. The cowl shock interacts with the expansion waves originating from the bodyside wall near the separated flow region. This creates complicated shock reflections inside the internal compression region. Further, the variation of shock structures in two lateral planes is evident that the flow is highly complex and three-dimensional inside the engine.

The Mach contour obtained at two lateral stations  $z/h = 0.1$  and  $z/h = 0.46$  are shown in Fig. 9. The boundary layer growth on the bodyside wall is seen from both the sections. A low Mach number region is observed at the bodyside wall in the external compression region. This results from a abrupt change in flow direction at the  $5^\circ$  compression ramp. The deceleration of the free stream flow and the pressure recovery resulting from two external compression ramp, internal compression, and the oblique shock emanating from cowl lip are also seen from these contours.

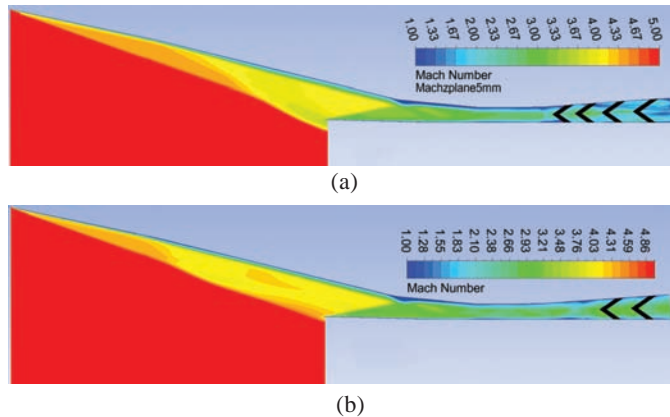


Figure 9. Mach number distribution at ; (a)  $z/h=0.1$  and (b)  $z/h = 0.46$ .

The streamlines entering into the internal compression region are shown in Fig. 10. These are used for finding the existence of the bubble inside the intake. It is clearly seen from these plots that the re-circulating zone is presents on the bodyside wall.

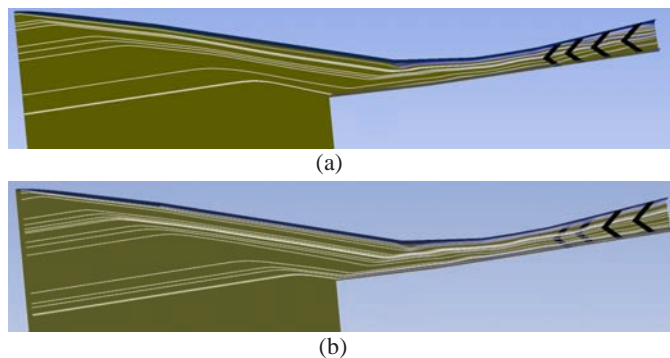


Figure 10. Streamline plot at (a)  $z/h=0.1$ , (b)  $z/h=0.46$  planes.

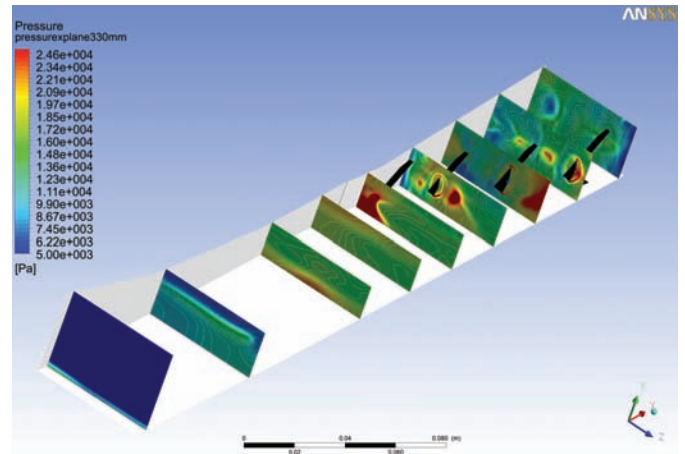


Figure 11. Pressure distribution across the flow path at different axial stations.

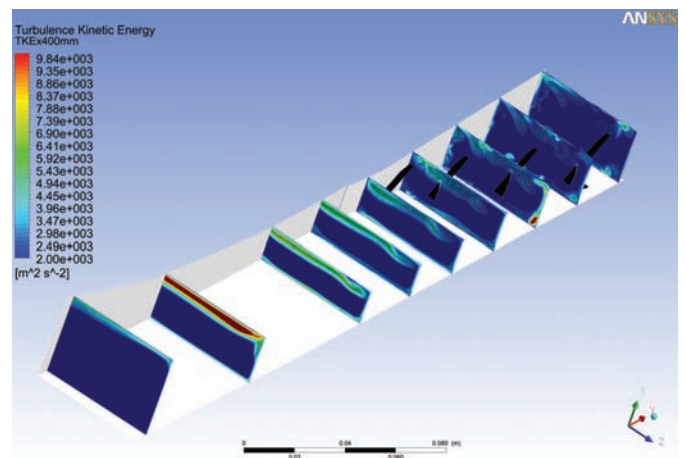


Figure 12. TKE distribution at different axial locations.

### 4.4 Sectional Variation of Pressure and Turbulence Kinetic Energy

The pressure contours and turbulence kinetic energy distribution at various sections along the axial direction are shown in Figs 11 and 12. The results are presented at the following locations:  $x/h = 6.3, 7.8, 9.3, 10, 10.6, 11.1, 11.7, 12.3,$  and  $12.9$ . The shock originated from the cowl-leading edge, middle wall and at the struts is seen clearly from Fig.11. At  $x/h = 6.3$ , a thick line shows the near two-dimensional oblique shock originating from the cowl-leading edge. The occurrence of low-energy fluid occupying a considerable segment of the intake cross-sectional area is seen at around  $x/h = 7.8$ . This degrades the performance of the intake and it is resulting from the separation of flow in the bodyside of internal ramp. A significant pressure rise at the entry and at the exit plane-of the isolator ( $x/h = 9.3$  and  $10$ ) is due to multiple shock reflections at the bodyside and cowlside walls. The presence of finite thickness middle wall and its leading edge causes a strong pressure rise at  $x/h = 10.6$  on the cowl side wall. However, it is reduced at the bodyside wall due to flow expansion in the second divergence of the combustion chamber.

The production of turbulence kinetic energy at different axial locations  $x/h = 6.3, 7.8, 9.3, 10, 10.6, 11.1, 11.7, 12.3,$

and 12.9 are presented in Fig. 12. This plot indicates the loss in kinetic energy along the flow direction. A significant increase in TKE is observed at  $x/h=6.3$  on the bodyside wall. This is due to the origination of boundary layer from the nose tip of the body. Another sharp rise in TKE is observed at  $x/h = 7.8$  where the separation bubble was observed. This minimizes the core area of the flow passage and reduces the mass capture significantly. The flow separation zone is to be minimised through various boundary layer control techniques or through geometry optimisation so as to improve the starting and performance characteristics of the intake.

**4.5 Total Pressure Recovery**

The total pressure through the scramjet engine changes due to several parameters. The total pressure recovery (TPR) is used for characterising the performance of the engine. It measures the amount of free-stream flow conditions that are recovered and it is as a ratio of total pressure at any station divided by the free-stream total pressure. It depends on a wide variety of factors, including the shape of the inlet, the speed of the aircraft, aircraft manoeuvres, boundary layer growth, flow separation, shocks, and shock-shock and shock boundary layer interactions. Figure 13 shows the TPR along the flow path at various heights from the bodyside wall at the middle plane of the four struts. The constant area section between internal compression section and combustor is defined as isolator.  $h_{iso}$  denotes the height of the isolator which is equal to  $0.3h$  (ref. Fig. 1). The TPR close to the bodyside wall reduces continuously due to the growth of the boundary layer ( $1/8$  and  $1/4$  of  $h_{iso}$ ). The separated flow region on the bodyside wall is clearly seen at  $x/h=7.4$  from large reduction in TPR. The TPR is less than 10 per cent in the separated zone. It is more than 70 per cent away from the bodyside wall in the external intake. A continuous reduction in TPR is observed inside the internal compression ramp, isolator, and the combustion chamber due to shocks and shock boundary layer interactions.

The area-averaged TPR at the entry of the internal compression ramp is 59.6 per cent. It is reduced to 31.7 per cent

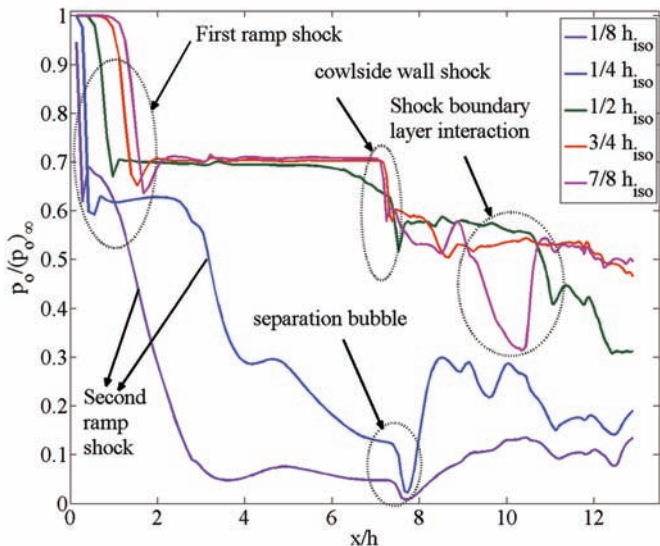


**Figure 13. Total pressure recovery along the flow path at various heights.**

at the combustion chamber inlet due to losses in internal compression ramp and at the isolator. The total mass flow entering through the forebody of the vehicle is  $0.148 \text{ kg/m}^3$ . It is around  $0.138 \text{ kg/m}^3$  at the entrance of the internal compression region. This value of mass flow rate is verified with calculations made at two locations inside the scramjet engine. The mass capture ratio is defined as a ratio of mass flow rate at the intake entry to the mass flow captured at the free stream. It is found that the mass capture ratio is 93.3 per cent for the present configuration.

**5. CONCLUSIONS AND FUTURE WORK**

Three-dimensional simulations have been performed on a mixed compression scramjet intake integrated with the conceptual hypersonic vehicle for a free-stream Mach number of 6 with  $5^\circ$  angle-of-attack using ANSYS CFX software by solving the Navier-Stokes equations with the SST turbulence model. The detailed flow field at the hypersonic mixed compression intake, isolator, and combustion chamber have been analysed. The following conclusions have been made based on the computational analysis:

- The wall pressure obtained from the simulation matches reasonably well with the experimental data. This showed that the present simulation is convincingly capable of predicting the strong secondary flows and the three-dimensional shock boundary layer interactions present in the hypersonic intakes.
- A flow separation zone at the bodyside wall has been identified which minimizes the effective core area of the flow passage and reduces the mass capture significantly. This may be minimised through various boundary layer control techniques (such as suction, blowing, plasma, and porous wall) or through geometry optimisation so as to improve the starting and performance characteristics of the intake.
- The re-circulation zones behind the struts have also been identified. These zones are formed due to the interaction of the struts shocks with the middle wall shocks. These regions may be chosen for injecting fuel so as to get better mixing of fuel and air.
- The total pressure recovery is as low as 10 per cent in the separated flow region and the area averaged total pressure recovery at the entry of the combustor is 32 per cent.
- The mass flow rate at the internal compression entry plane is  $0.138 \text{ kg/m}^3$ . The mass capture ratio is found to be 93.3 per cent for the present configuration under the computed free-stream conditions.

Finer grids near the wall surfaces may reveal the detailed flow structures responsible for sharp variations in pressure and the recirculation bubble strength accurately. This will be examined in future.

**REFERENCES**

1. Heiser, W.H.; Pratt, D.T.; Daley, D.H. & Mehta, U.B. Technical background. *In* Hypersonic Air-breathing propulsion. AIAA Inc., Washington, 1994. pp. 29-52.
2. Roy, M. Thermodynamique des Systemees Propulsifs a Reaction. *DUNOD*, Paris, France, 1947.

3. Ferri, A. Possible directions of future research in air-breathing engines. 4<sup>th</sup> AGARD Combustion and Propulsion Colloquium. Pergamon Press Ltd, London, England, 1960, pp. 16-36.
4. McClinton, C.R.; Andrews, E.H. & Hunt, J.L. Engine development for space access: Past, present and future. International Symposium on Air Breathing Engines, 2001, Paper 2001-1074.
5. Curran, E.T. Scramjet engines: The first forty years. *J. Propuls. Power*, 2001, 17(6), 1138. doi: 10.2514/2.5875
6. Fry, R.S. A century of ramjet propulsion technology evolution. *J. Propuls. Power*, 2004, 20(1), 27-58. doi: 10.2514/1.9178
7. Panneerselvam, S; Thiagarajan, V; Ganesh T.K; Justina Geetha, J; Ramanugachari, V & Prahlada. Airframe integrated scramjet design and performance analysis. XVII International Symposium on Air Breathing Engines (17<sup>th</sup> ISOABE), Munich, Germany, 2005.
8. Tahir, R. Analysis of shock dynamics in supersonic intakes. McGill University, Montreal, 2008, 1-21. (PhD Thesis)
9. Bissinger, N.C.; Blagoveshchensky, N.A.; Gubanov, A.A.; Gusev, V.N.; Starukhin, V.P.; Voevodenko, N.V. & Zadonsky, S.M. Improvement of forebody/inlet integration for hypersonic vehicle. *Aerospace Sci. Techno.*, 1998, 2(8), 505-514. doi: 10.1016/S1270-9638(99)80009-1
10. Smart, M.K. Experimental testing of a hypersonic inlet with rectangular-to-elliptical shape transition. *J. Propuls. Power*, 2001, 17(2), 276-283. doi: 10.2514/2.5774
11. Kantrowitz, A. & Donaldson, C. Preliminary investigation of supersonic diffusers. NACA WR L-713, 1945.
12. Parikh, P.; Engelund, W.; Armand, S. & Bittner, R. Evaluation of a CFD Method for aerodynamic database development using the hyper-X stack configuration. In 22<sup>nd</sup> Applied Aerodynamics Conference and Exhibit, August 2004, Paper no: AIAA 2004-5385.
13. Lanson, F. & Stollery, J.L. Some hypersonic intake studies. *Aeronautical J.*, 2006, Paper no: 2972, 145-156.
14. Sivakumar, R. & Babu, V. Numerical simulations of flow in a 3-D supersonic intake at high mach numbers. *Def. Sci. J.*, 2006, 56(4), 465-476. doi: 10.14429/dsj.56.1912
15. Saha, S. & Chakraborty, D. Hypersonic Intake starting characteristics—A CFD validation study. *Def. Sci. J.*, 2012, 62(3), 147-152. doi: 10.14429/dsj.62.1340
16. Van Wie, D.M. & Ault, D. Internal flow field characteristics of a scramjet inlet at Mach 10. *J. Propuls. Power*, 1996, 12, 158–164. doi: 10.2514/3.24005
17. Tan, H.; Sun, S. & Huang, H. Behavior of shock trains in a hypersonic inlet/isolator model with complex background waves. *Exp. Fluids*, 2012, 53, 1647–1661. doi: 10.1007/s00348-012-1386-1
18. Smart, M.K. How much compression should a scramjet inlet do? *AIAA Journal*, 2012, 50, 610–619. doi: 10.2514/1.J051281
19. Gruhn, P.; Gülhan, A. Experimental investigation of a hypersonic inlet with and without sidewall compression. *J. Propuls. Power*, 2011, 27, 718–729. doi: 10.2514/1.50347
20. Idris, A.C; Saad, M.R; Zare-Behtash, H. & Kontis, K. Luminescent measurement systems for the investigation of a scramjet inlet-isolator. *Sensors*, 2014, 14, 6606-6632. doi: 10.3390/s140406606
21. Panneerselvam, S.; Ganesh, T.K.; Justina Geetha, J.; Thiagarajan, V. & Balu, G. Flow path design of a vehicle integrated hydrocarbon based dual mode ramjet/scramjet engine. In AIAA/AAAF 11<sup>th</sup> International Space Planes and Hypersonic Systems and Technologies Conference, France, AIAA-2002-5215, 2002.
22. ANSYS CFX Reference guide, Release 14.0, ANSYS, Inc. 2011.
23. Menter, F.R. Two-equation eddy-viscosity turbulence models for engineering applications. *AIAA Journal*, 1994, 32(8). doi: 10.2514/3.12149
24. Wilcox, D.C. Formulation of the k- $\omega$  turbulence model revisited. In 45<sup>th</sup> AIAA Aerospace Sciences Meeting and Exhibit, AIAA Paper 2007-1408, Reno, Nevada, 2007.
25. Wilcox, D.C. Turbulence modelling for CFD. 2<sup>nd</sup> Ed., DCW industries, 1998.

#### ACKNOWLEDGEMENTS

The authors gratefully acknowledge the High Performance Computing Facility at CSIR-Central Mechanical Engineering Research Institute (CMRI), Durgapur for providing the necessary computational resources. And Mr Anupam Sinha, Aerosystems Laboratory, CSIR-CMERI for providing the solid modelling drawing to generate grid.

#### CONTRIBUTORS

**Dr T. Murugan** received his BTech (Aeronautical Engg) from Madras Institute of Technology, Anna University, Chennai, in 2001. He has pursued his M.Tech and PhD in Aerospace Engineering from Indian Institute of Technology, Kanpur. He joined CSIR-Central Mechanical Engineering Research Institute (CMERI), Durgapur in 2010. His research interests are shock tube flows, computational fluid dynamics of compressible flows, experimental aerodynamics and drag reduction.

**Dr Sudipta De** received his BTech and MTech in Mechanical Engineering and Heat Power Engineering from B.E. College, Howrah. He obtained his PhD (Aerospace Engineering) from Indian Institute of Technology, Kanpur in 2005. He joined CSIR-Central Mechanical Engineering Research Institute (CMERI), Durgapur in 2009. His major scientific interests are computational fluid dynamics, compressible flows and vorticity dynamics.

**Dr V. Thigarajan** received his BTech (Aeronautical Engg) from Madras Institute of Technology, Chennai and M.E (Aerospace Engineering) from Indian Institute of Science, Bangalore. He obtained his PhD degree in Aerospace Engineering from Indian Institute of Technology, Kanpur in 2007. He joined Defence Research and Development Laboratory, Hyderabad in 1992. He has designed and developed air-intake system and experimentally characterised the same through wind tunnel testing at hypersonic Mach numbers at TsAGI, Russia for the Hypersonic Technology Demonstration Vehicle which is an ongoing project at DRDL. His research interests are aerodynamic design of missiles and intake for hypersonic air-breathing vehicle.